

# Local density dependent potential for compressible mesoparticles

G r me Faure and Jean-Bernard Maillet  
*CEA, DAM, DIF, F-91297 Arpajon, France*

Gabriel Stoltz  
*Universit  Paris-Est, CERMICS (ENPC), INRIA, F-77455 Marne-la-Vall e, France*  
(Dated: July 23, 2018)

We focus on finding a coarse grained description able to reproduce the thermodynamic behavior of a molecular system by using mesoparticles representing several molecules. Interactions between mesoparticles are modelled by an interparticle potential, and an additional internal equation of state is used to account for the thermic contribution of coarse grained internal degrees of freedom. Moreover, as strong non-equilibrium situations over a wide range of pressure and density are targeted, the internal compressibility of these mesoparticles has to be considered. This is done by introducing a dependence of the potential on the local environment of the mesoparticles, either by defining a spherical local density or by means of a Voronoi tessellation. As an example, a local density dependent potential is fitted to reproduce the Hugoniot curve of a model of nitromethane, where each mesoparticle represents one thousand molecules.

## I. INTRODUCTION

Since two decades, the development of coarse graining strategies from all-atoms classical molecular dynamics (MD) to the mesoscale has known a continuous growing interest. This is particularly relevant for complex systems where longer time and length scales behaviors should be addressed. A first step toward the development of reduced models was the idea of united atoms potentials, where some atoms belonging to the same molecule are considered as a single center of force, without any modification of the equations of motion (EoM). A general framework for coarse graining which employs modified EoM appeared with the Dissipative Particle Dynamics (DPD) method [1], where a particular mesoscopic model can be deduced from its atomistic representation [2]. In this method, coarse grained degrees of freedom are introduced, the effect of the lost degrees of freedom being modelled by the addition of dissipative and stochastic terms in the EoM. A relation between the amplitude of fluctuations and dissipation guaranties that the canonical distribution is sampled [3]. DPD has finally become a standard method to simulate complex fluids at the mesoscale, and is generally associated with soft potentials allowing to use larger integration timesteps. However, for target simulations in the microcanonical ensemble (NVE) or for non-equilibrium situations, an additional variable has to be introduced to guaranty the conservation of the total energy [4–7], leading to DPD with conserved energy (DPDE). This is particularly useful in the case of shock wave simulations, where the equilibrium temperature in the shocked state relies on the ability of the molecule to store energy, as the kinetic energy is split between intermolecular (i.e. center of mass motion) and intramolecular (vibrons) motions. For complex large molecules, the intramolecular part is the dominant term. The additional variable, the internal energy of the mesoparticle, is linked to the internal temperature through an internal equation of state ( $\epsilon = \int C_v(T)dT$ ). The heat capacity  $C_v(T)$  rep-

resents the thermic contribution of the internal coarse-grained degrees of freedom. DPDE allows to reproduce thermodynamic properties of molecular systems over a wide range of pressures and densities, as well as non-equilibrium shock wave situations. One hidden approximation during this coarse graining of a molecule to a mesoparticle is the implicit hypothesis of the rigidity of the molecule, i.e., the molecule is not compressible at all, and only thermic effects have been considered so far. This hypothesis is no longer valid when several molecules are represented by a single mesoparticle: the compressibility of this ensemble of molecule is obviously not null (and eventually tends to the compressibility of the whole system when mesoparticles get larger). Such "internal" compressibility can be accounted for by introducing a dependence of the parameters of the effective interaction potential on the local density.

Density dependent potentials (DDP) have been widely used in the literature, aiming originally at modelling specific effects as for example the bonding directionality for covalent materials with the Tersoff potentials [8], or metallic bonding using the embedded atom method [9]. One has to distinguish between global and local density dependent potential, and be aware that there is not a unique way to fit their parameters [10]. Nevertheless, DDP have received renewed attention in the last few years, particularly to assess the question of transferability of the potential and to gain accuracy in the prediction of thermodynamic properties[11–13]. The main concern here is the transferability of the potential over a wide range of pressures and densities. To this aim, we present in this article a model of compressible mesoparticles using local density dependent potentials.

## Outline

This article is organized as follows. We first recall in Section II two approaches to defining a local density: either through some local spherical averages (Section II A) or using Voronoi cells to define a local volume (Section II B). It turns out that both approaches lead to very different results, as carefully documented in Section II C. We therefore favor the Voronoi approach since it is, as we argue, more transferable with respect to modifications of the local thermodynamic conditions. In a second step, we describe in Section III the density dependent potentials we use, and discuss their tendency to (strongly) alter the average pressure in the system. Finally, as a stringent application, we reproduce the Hugoniot curve of a nitromethane like material in Section IV.

## II. DEFINING A LOCAL DENSITY

### A. Locally averaged density

Consider an ensemble of  $N$  (meso)particles of mass  $m$  located at positions  $\{q_i\}_{i=1,\dots,N}$ . The standard approach to define a continuous density field from this discrete set of masses is to use weight functions centered around particle centers. We consider a smooth, non negative, spherically symmetric function  $\chi$  vanishing for  $r \geq r_{\text{cut}}$ . Denoting by  $r_{i,j} = |q_i - q_j|$  the distance between two particles, the local density  $\rho_i^s$  of particle  $i$  reads

$$\rho_i^s = \frac{1}{4\pi} \frac{\sum_{j=1}^N m \chi(r_{i,j})}{\int_0^{r_{\text{cut}}} \chi(r) r^2 dr}. \quad (1)$$

We consider in the sequel three examples of weighting function:

- a third order spline function  $\chi_{\text{sp}}$  such that  $\chi_{\text{sp}}(0) = 1$ ,  $\chi_{\text{sp}}(r_{\text{cut}}) = 0$  and  $\chi'_{\text{sp}}(0) = \chi'_{\text{sp}}(r_{\text{cut}}) = 0$ ;
- a smoothed step function  $\chi_{\text{ssf}}$  such that  $\chi_{\text{ssf}}(r) = 1$  for  $r < 0.9 r_{\text{cut}}$ , which is smoothly going down to 0 for  $0.9 r_{\text{cut}} \leq r \leq r_{\text{cut}}$  (thanks to a cubic spline);
- the Lucy function, commonly used in SPH models [14]

$$\chi_{\text{lf}}(r) = \left(1 + 3 \frac{r}{r_{\text{cut}}}\right) \left(1 - \frac{r}{r_{\text{cut}}}\right)^3.$$

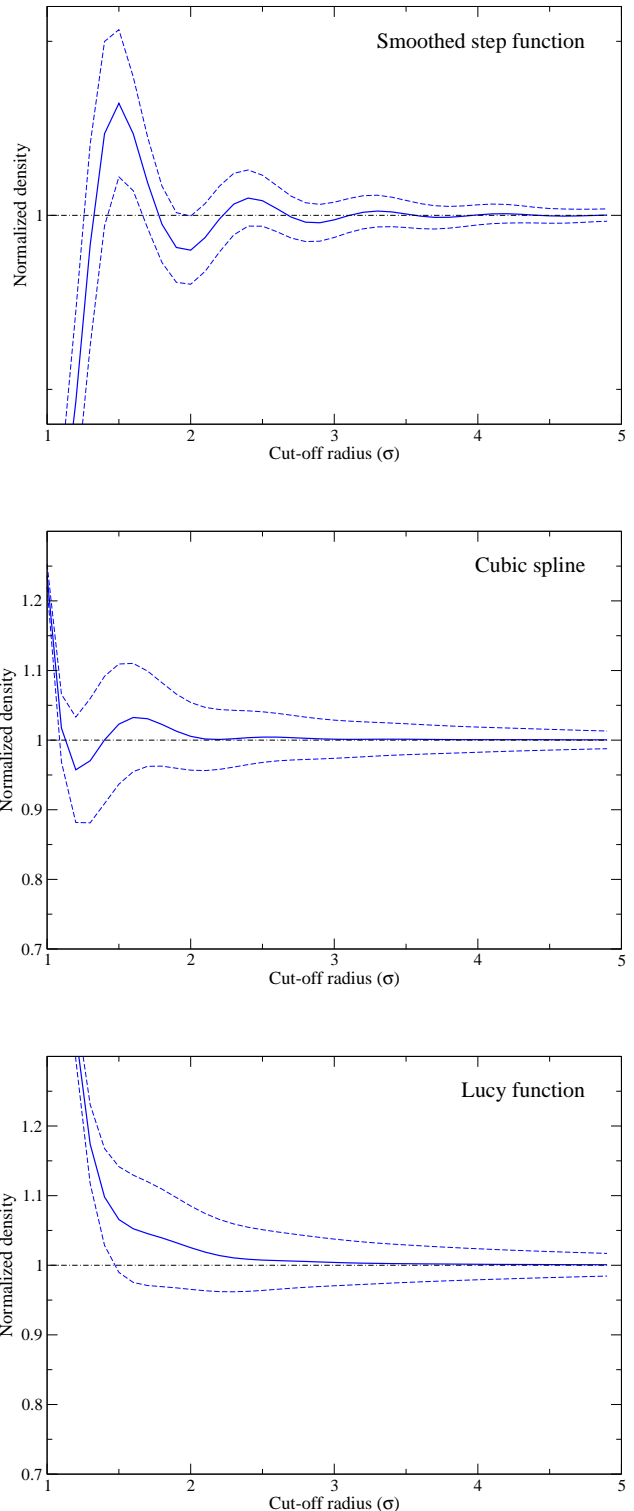


FIG. 1: Mean local density  $\frac{\langle \rho^s \rangle}{\rho_{\text{th}}}$  (solid line), and the envelop corresponding to the standard deviation of the distributions of densities (dashed lines) with respect to the cut-off radius  $r_{\text{cut}}$ . Top: smoothed step function  $\chi_{\text{ssf}}$ . Middle: cubic spline  $\chi_{\text{sp}}$ . Bottom: Lucy function  $\chi_{\text{lf}}$ .

The definition of the local densities crucially depends on the choice of the weight function and of its cut-off radius. The mean local density  $\langle \rho^s \rangle$ , computed by averaging the local densities  $\{\rho_i^s\}_{i=1,\dots,N}$  using the arithmetic average

$$\langle \rho^s \rangle = \frac{1}{N} \sum_{i=1}^N \rho_i^s, \quad (2)$$

is plotted as a function of the cut-off radius  $r_{\text{cut}}$  for the previously defined weight functions in Figure 1. The simulation is performed for Argon at temperature  $T = 300$  K and density  $\rho_{\text{th}} = 1650 \text{ kg}\cdot\text{m}^{-3}$ . Argon is described by a Lennard-Jones potential with parameters  $\sigma = 3.4 \text{ \AA}$  and  $\varepsilon/k_B = 120$  K, truncated at  $r_{\text{LJ}} = 2.5\sigma$ . In all this work, constant temperature simulations are performed in the NVT ensemble, which is sampled with a Langevin dynamics (the integrator we use and the parameters of the dynamics are described in Appendix A).

Figure 1 shows that the thermodynamic density  $\rho_{\text{th}}$  and the mean local density  $\langle \rho^s \rangle$  agree for large cut-off radii, as expected since local environment effects are averaged out. On the other hand, too small a radius causes large discrepancies between  $\rho_{\text{th}}$  and  $\langle \rho^s \rangle$  due to the structure of the radial distribution function. This suggests to consider large radii in order to avoid systematic biases in the simulation. However, this option is expensive, and suppresses any information on the density variations.

We have checked that other averages, for instance, harmonic averages, also lead to biased mean spherical densities (see Appendix B).

The bias in the mean local density is often removed by renormalizing the local densities as  $\rho_i^s \frac{\rho_{\text{th}}}{\langle \rho^s \rangle}$ , or by computing the theoretical mean local density at  $r_{\text{cut}}$  given an a priori equation of state [15]. These remedies however hide the actual issue at stake, namely model inconsistency. In any case, local density averages cannot be applied to the simulation of shock compressions where the density is a priori unknown and strongly inhomogeneous in non-equilibrium systems.

## B. Voronoi tessellation

An alternative way to define local densities is to introduce a local notion of volume associated with a particle. In order to recover the thermodynamic density in average, we use a partitioning of the total volume using the particle centers as reference points to construct a Voronoi tessellation. This is a standard approach in mesoscale models of dissipative particle dynamics [16]. However, the equations governing the evolution of these models are of hydrodynamic type, with postulated equations of states. In contrast, the model we consider in this article is still of atomistic nature, with particles interacting through potential energy functions.

We denote by  $R_i$  the Voronoi cell associated with the  $i$ th particle (defined as the set of points closer to  $q_i$  than

any other particle  $q_j$ , see Figure 2), and by  $V_i = |R_i|$  its volume. The local density is defined as

$$\rho_i^v = \frac{m}{V_i},$$

while the average density  $\bar{\rho}^v$  in the system is defined through the harmonic average

$$\frac{1}{\bar{\rho}^v} = \frac{1}{N} \sum_{i=1}^N \frac{1}{\rho_i^v}.$$

Since the Voronoi tessellation defines a partition of the space (of total volume  $V_{\text{tot}}$ ), we automatically have  $\sum V_i = V_{\text{tot}}$ , thus  $\bar{\rho}^v = \rho_{\text{th}}$ . Besides, the Voronoi volume does not depend on a weight function or a parameter such as a cut-off radius, which is a clear advantage to unambiguously define a local density.

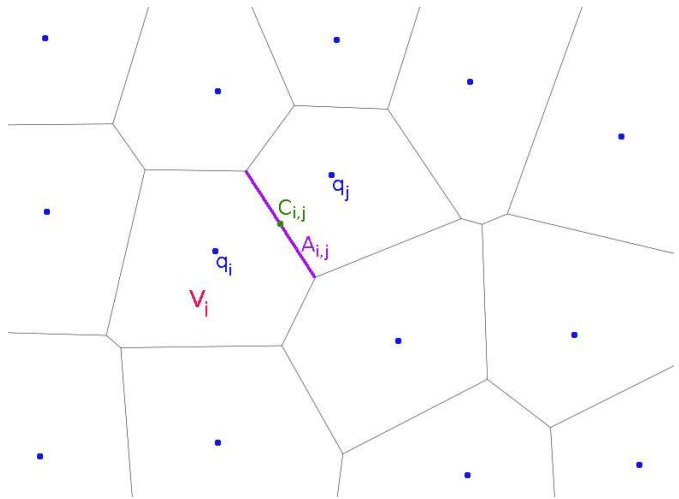


FIG. 2: A 2D Voronoi tessellation. Two cells  $R_i, R_j$ , of respective centers  $\mathbf{q}_i, \mathbf{q}_j$  and volumes  $V_i, V_j$  are highlighted. The area of the surface separating these cells is denoted  $A_{i,j}$ ,  $\mathbf{C}_{i,j}$  being the centroid of the corresponding face.

Since we aim at performing molecular dynamics with interaction potentials depending on the local density, hence on the Voronoi volumes, the derivatives of the volumes  $V_i$  with respect to the particle positions are needed. As shown in [17], it holds, for  $j \neq i$ ,

$$\nabla_{\mathbf{q}_j} V_i = -\frac{A_{i,j}}{r_{i,j}} (\mathbf{C}_{i,j} - \mathbf{q}_j), \quad (3)$$

where  $A_{i,j}$  and  $\mathbf{C}_{i,j}$  are respectively the area and the centroid of the face of the Voronoi diagram between cells  $i$  and  $j$ . The derivative with respect to the position of particle  $i$  can easily be inferred from the other derivatives given in (3) by using the invariance of the Voronoi volume with respect to a translation, which implies

$$\sum_j \nabla_{\mathbf{q}_j} V_i = 0. \quad (4)$$

Let us also recall an interesting property of the Voronoi volumes under dilation or compression, which is useful to understand average pressures in materials described by density dependent potentials (see Section III B):

$$\sum_j (\nabla_{\mathbf{q}_j} V_i) \cdot \mathbf{q}_j = 3V_i. \quad (5)$$

### C. Comparison of the spherical and Voronoi densities

We now investigate the relationship between the two notions of local density defined in Sections II A and II B. We expect particles with high spherical local densities to have small Voronoi volumes. On the other hand, since the local density  $\rho_i^s$  is computed from the positions of all the particles within a certain radius, it is unclear whether it agrees with the Voronoi densities, which depend only on the nearest neighbors.

Figure 3 presents a histogram of the Voronoi and spherical densities (with  $r_{\text{cut}} = r_{\text{LJ}}$  for the latter one) in the NVT ensemble at  $T = 300$  K and  $\rho_{\text{th}} = 1650 \text{ kg.m}^{-3}$ , using a Lennard-Jones potential for Argon. Both can reasonably be considered as Gaussian. We find here a standard deviation of  $0.0854\rho_{\text{th}}$  for the Voronoi density. The standard deviation of the spherical density depends on the cut-off radius as Figure 1 suggests. At  $r_{\text{cut}} = 2.5\sigma$ , it is smaller than the variance of the Voronoi volume and equal to  $0.0359\rho_{\text{th}}$ .

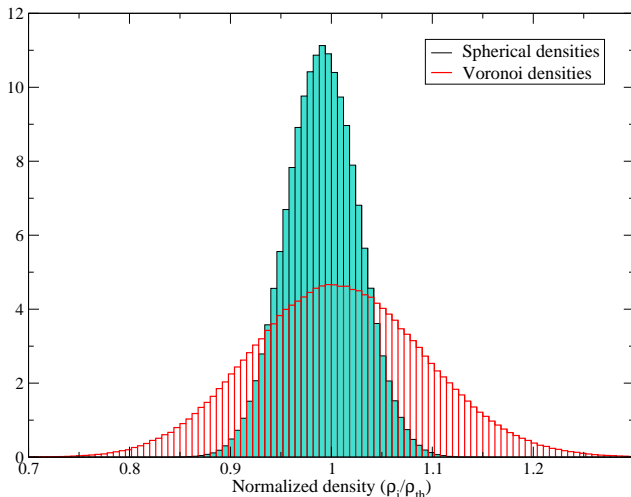


FIG. 3: Distribution of the spherical ( $r_{\text{cut}} = 2.5\sigma$ ) and Voronoi densities at  $\rho = 1650 \text{ kg.m}^{-3}$

In order to more quantitatively compare the two notions of densities, we next compute the correlation between normalized densities. We introduce to this end the standard deviation for the spherical densities using

the arithmetic average (2):

$$\text{sd}(\rho^s) = \sqrt{\frac{1}{N} \sum_{i=1}^N (\rho_i^s - \langle \rho^s \rangle)^2},$$

and similarly for the Voronoi densities

$$\text{sd}(\rho^v) = \sqrt{\frac{1}{N} \sum_{i=1}^N (\rho_i^v - \langle \rho^v \rangle)^2}.$$

We then consider the normalized densities  $\tilde{\rho}_i^s$  and  $\tilde{\rho}_i^v$ , which have mean 0 and variance 1, namely

$$\tilde{\rho}_i^s = \frac{\rho_i^s - \langle \rho^s \rangle}{\text{sd}(\rho^s)}, \quad \tilde{\rho}_i^v = \frac{\rho_i^v - \langle \rho^v \rangle}{\text{sd}(\rho^v)},$$

and compute the correlation

$$C = \frac{1}{N} \sum_{i=1}^N \tilde{\rho}_i^s \tilde{\rho}_i^v. \quad (6)$$

As demonstrated by Figure 4, the correlation is quite high when the cut-off radius of the spherical averages is small (*i.e.* when the same neighbors are taken into account). It however varies in a non-monotonic way, first decreasing until  $r_{\text{cut}} \simeq 1.7\sigma$ , then increasing again until  $r_{\text{cut}} \simeq 2.2\sigma$ , and still oscillating for larger radii. In any case, the correlation remains quite small.

We investigate more precisely the relationship at the important values  $r_{\text{cut}} = 2.5\sigma$  (which is also the potential energy cutoff  $r_{\text{LJ}}$ ) and  $r_{\text{cut}} = 1.2\sigma$  (where the correlation is maximum), by plotting in Figure 5 the joint distribution of  $(\tilde{\rho}_i^s, \tilde{\rho}_i^v)$ . The correlation in the case  $r_{\text{cut}} = 2.5\sigma$  is close to 0, which is indicated by the absence of trend in the joint distribution, in sharp contrast with the joint distribution at  $r_{\text{cut}} = 1.2\sigma$ .

## III. INTRODUCING A LOCAL DENSITY DEPENDENCE IN THE POTENTIAL

We present in this section a possible density dependent potential to be used in conjunction with a definition of local densities based on a Voronoi tessellation. We carefully study the average pressure computed from the corresponding physical model. Let us indeed insist that, to properly simulate and predict the behavior of materials under shock compressions, the equation of state needs to be correctly described.

### A. Definition of a local density dependent potential

We present in this section a way to incorporate local density effects in the interaction potential. We consider systems with pairwise forces, such as exp-6 or Lennard-Jones, and denote the interaction energy between two

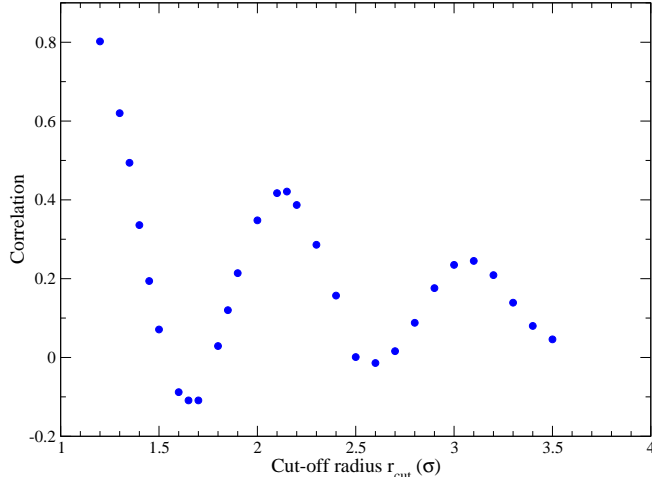


FIG. 4: Correlation (6) between the Voronoi and local densities with respect to the local density cut-off radius  $r_{\text{cut}}$ .

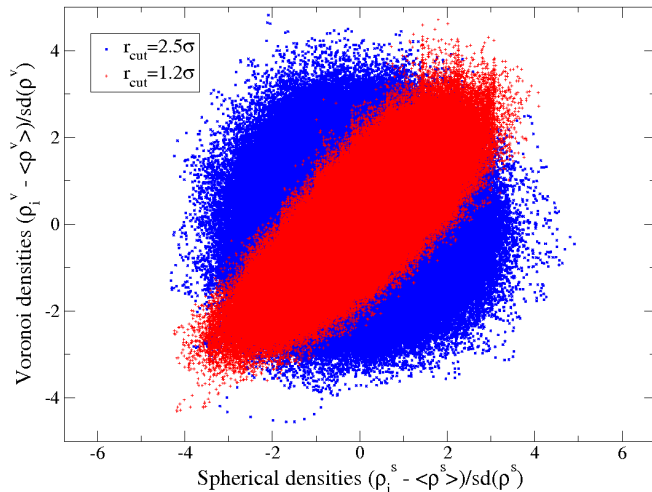


FIG. 5: Joint distribution of the Voronoi and spherical densities at  $r_{\text{cut}} = 1.2\sigma$  (red) and  $r_{\text{cut}} = 2.5\sigma$  (blue).

particles  $i$  and  $j$  by  $\mathcal{U}_{\text{std}}(r_{i,j})$ . One possible choice is to correct the distance  $r_{i,j}$  between the particle centers to account for local density effects, by replacing  $r_{i,j}$  by  $r_{i,j} - \lambda_{i,j}$  with

$$\lambda_{i,j} = \lambda(V_{i,j}), \quad V_{i,j} = \frac{V_i + V_j}{2}.$$

The associated interaction energy (density dependent potential  $\mathcal{U}_{\text{dd}}$ ) reads

$$\mathcal{U}_{\text{dd}}(r_{i,j}, V_{i,j}) = \mathcal{U}_{\text{std}}(r_{i,j} - \lambda_{i,j}), \quad (7)$$

so that the total potential energy is

$$\mathcal{U}_{\text{tot}}(q_1, \dots, q_N) = \sum_{1 \leq i < j \leq N} \mathcal{U}(r_{i,j} - \lambda_{i,j}).$$

The physical idea underpinning the choice of the correction  $\lambda_{i,j}$  is that the interactions between mesoparticles arise from the individual interactions of the atoms or molecules represented by the mesoparticles. This interaction should be dominated by atoms or molecules on the surface of the mesoparticles. We therefore need to use  $r_{i,j} - \lambda_0$  as the interaction distance at some density  $\rho_0$ , with  $\lambda_0 \geq 0$  representing the size of the mesoparticle. When the density increases, the distance between the centers of the mesoparticles decreases but their sizes should also decrease to mimic their internal compressibility. Hence the correction  $\lambda$ , i.e. the mesoparticle diameter, should decrease as the density increases (or equivalently  $\lambda$  should be an increasing function of the voronoi volume).

In fact, this can be seen as a way of correcting the interaction distance to take into account the compressibility of the mesoparticles to prevent the system from becoming too stiff (see Figure 6).

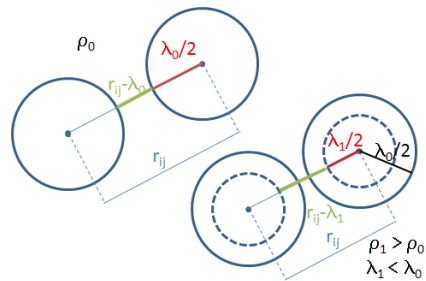


FIG. 6: Correction of the density effect on the interaction distance.

Another way to introduce a density dependence is discussed in Appendix C. The approach described there essentially consists in assigning effective volumes to the particles depending on the local density.

Although obvious, it is worth emphasizing that the dependence of the volumes  $V_i, V_j$  on the particle positions induces extra terms in the expressions of the atomic forces as compared to the forces arising from the standard potential  $\mathcal{U}_{\text{std}}$ . More precisely,

$$\begin{aligned} \mathbf{F}_{\text{dd}}^{i,j,k} &= -\nabla_{\mathbf{q}_k} \mathcal{U}_{\text{dd}}(r_{i,j}, V_{i,j}) \\ &= ((\delta_{k,i} - \delta_{k,j}) \mathbf{e}_{i,j} + \lambda'(V_{i,j}) \nabla_{\mathbf{q}_k} V_{i,j}) \mathcal{U}'_{\text{std}}(r_{i,j} - \lambda_{i,j}) \end{aligned} \quad (8)$$

where  $\mathbf{e}_{i,j} = (q_j - q_i)/r_{i,j}$ .

## B. Analytic calculation of the virial pressure for density dependent potentials

We show in this section that the pressure computed with density dependent potentials may be very different from the one computed with standard potentials. We focus on the potential part of the pressure, by considering the so-called virial pressure

$$P_{\text{pot}}(q) = -\frac{1}{3V_{\text{tot}}} \sum_{k=1}^N \mathbf{q}_k \cdot \nabla_{\mathbf{q}_k} \mathcal{U}_{\text{tot}} = \frac{1}{3V_{\text{tot}}} \sum_{1 \leq i < j \leq N} w_{\text{dd}}^{i,j},$$

with

$$w_{\text{dd}}^{i,j} = -\sum_{k=1}^N \mathbf{q}_k \cdot \nabla_{\mathbf{q}_k} \mathcal{U}(r_{i,j} - \lambda_{i,j}).$$

This expression should be compared to the contribution arising only from the direct pairwise interaction between  $i$  and  $j$ :

$$w_{\text{direct}}^{i,j} = -r_{i,j} \mathcal{U}'_{\text{std}}(r_{i,j} - \lambda_{i,j}).$$

The expression of the force (8) shows that  $w_{\text{dd}}^{i,j}$  is related to  $w_{\text{direct}}^{i,j}$  as:

$$w_{\text{dd}}^{i,j} = w_{\text{direct}}^{i,j} \left( 1 - \sum_{k=1}^N \frac{\lambda'(V_{i,j})}{r_{i,j}} \nabla_{\mathbf{q}_k} \left( \frac{V_i + V_j}{2} \right) \cdot \mathbf{q}_k \right).$$

Using (5), we finally obtain:

$$w_{\text{dd}}^{i,j} = w_{\text{direct}}^{i,j} \left( 1 - 3 \frac{\lambda'(V_{i,j}) V_{i,j}}{r_{i,j}} \right). \quad (9)$$

The variations of  $\lambda_{i,j}$  induce modifications to the global pressure compared to the case when  $\lambda$  is independent of the positions of the particles. As shown by the numerical experiments presented in Section III C, these modifications may be significant. As all thermodynamic and structural properties cannot be maintained accurately during the coarse graining process [18], we focus in the sequel on the pressure and specifically optimize the coarse grained potential to reproduce the pressure of the reference system.

## C. Numerical observations

We model the dependence of  $\lambda_{i,j}$  as a function of the Voronoi volumes for instance as

$$\lambda_{i,j} = S \left( \frac{V_{i,j}}{V_0} - 1 \right), \quad (10)$$

where  $S$  is a real parameter which can be positive or negative, and  $V_0$  is the average volume per particle  $V_{\text{tot}}/N$ . The reference situation corresponds to  $S = 0$ , in which case there is no density dependence in the interaction

potentials. Note that (10) ensures that the (arithmetic) average value  $\langle \lambda \rangle$  is always 0, whatever the value of  $S$ .

Our aim is to systematically study the average potential pressure as a function of the parameter  $S$  in (10). The Voronoi tessellation was implemented in 3D using the C++ library `Voro++` [19] with periodic boundary conditions. We use the potential from [20] as the standard potential  $\mathcal{U}_{\text{std}}$ , *i.e.*, an Exponential-6 potential :

$$\mathcal{U}_{\text{std}}(r) = \frac{\varepsilon}{\alpha - 6} \left( 6 \exp \left( \alpha \left[ 1 - \frac{r}{\sigma} \right] \right) - \alpha \left( \frac{\sigma}{r} \right)^6 \right). \quad (11)$$

The parameters set to  $\sigma = 4.5 \text{ \AA}$ ,  $\varepsilon/k_B = 427 \text{ K}$  and  $\alpha = 26$ . The values of these parameters are motivated by coarse-grained models of nitromethane where one particle stands for one molecule. The simulations were carried out in the NVT ensemble at room temperature ( $T = 300 \text{ K}$ ) and at a density chosen such that the average pressure vanishes ( $\rho_{\text{th}} = 1144 \text{ kg.m}^3$ ).

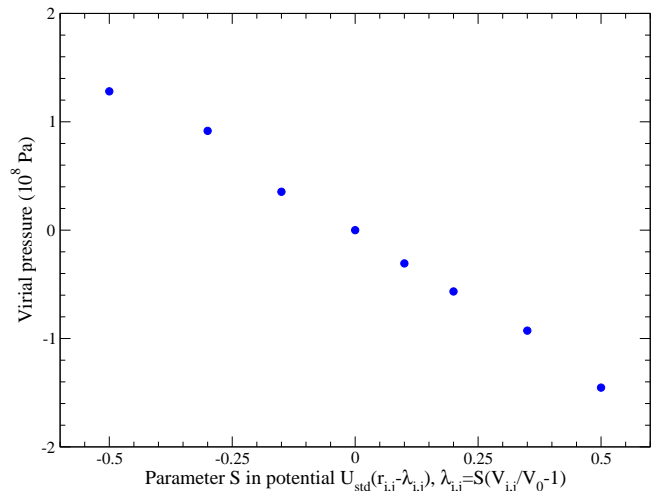


FIG. 7: Virial pressure computed for the Voronoi - dependent Exp-6 potential. The standard case corresponds to  $S = 0$ .

Whereas the kinetic pressure is of course the same in all these simulations, we plot in Figure 7 the total potential pressure for various values of  $S$ . The results show that genuinely density dependent potentials ( $S \neq 0$ ) lead to strong deviations of the potential pressure compared to the case  $S = 0$ . The sign of the deviation depends on the sign of  $S$ , in accordance with (9) since, in view of (10),

$$w_{\text{dd}}^{i,j} = w_{\text{direct}}^{i,j} \left( 1 - 3 \frac{S V_{i,j}}{V_0 r_{i,j}} \right).$$

The virial pressure is therefore increased when  $S < 0$ , and decreased when  $S > 0$ . Indeed,  $S > 0$  means that the diameter of the mesoparticle (*i.e.* proportional to  $\lambda$ ) decreases as its Voronoi volume decreases (or as its

local density increases), hence lowering the forces (and the pressure) between the mesoparticles. This is the expected physical behavior of the mesoparticle. On the contrary,  $S < 0$  means that  $\lambda$  is a decreasing function of the voronoi volume, meaning that the diameter of the mesoparticles increases as the density increases (hence increasing the pressure). This is an unwanted effect for physical applications.

#### IV. HUGONIOT CURVE FOR A MESOPARTICLE MODEL OF NITROMETHANE

We now turn to our main application, namely the computation of physical properties under strong regimes of pressure and temperature for models of mesoparticles. This is indeed a stringent test of the quality of the density dependent potentials suggested in Section III.

More precisely, we compute thermodynamic states along the Hugoniot curve for a model of mesoparticle representing 1,000 molecules of nitromethane ( $\text{CH}_3\text{NO}_2$ ). The molar mass of the mesoparticles is therefore 61 kg/mol. The potential energy function we use is the same as in Section III C, except that we change the parameters of the potential to  $\sigma = 9 \text{ \AA}$ ,  $\varepsilon/k_B = 300 \text{ K}$  and  $\alpha = 17$ . These parameters are obtained by fitting low density part of the Hugoniot curve. Reference data for Hugoniot curves are taken from the previous all-atom Monte Carlo simulations using a united atom model [21].

The important point to correctly reproduce the reference data is the functional form of the distance correction  $\lambda(V_{i,j})$ . We propose here a two step optimization method. We first consider in Section IV A a potential independent of the density, *i.e.*  $\lambda(V_{i,j}) = \lambda_0$  fixed. We determine the value of  $\lambda_0$  which reproduces the reference pressure  $P_{\text{th}}$  at each given thermodynamic density  $\rho_{\text{th}}$ . In a second step, we propose in Section IV B to fit the so-computed values of  $\lambda_0$  by linear or quadratic functions, and optimize upon the parameters in the fitting functions to fully reproduce the Hugoniot curve.

##### A. Suggested functional form of the distance correction

In order to have some data on how the distance correction  $\lambda$  may depend on the thermodynamic conditions, we first start by fitting its value on a series of  $N_{\text{ts}}$  thermodynamic states along the reference Hugoniot curve. We label these states by  $s$  and index them by their densities  $\rho_s$  and temperatures  $T_s$ . The optimal value of  $\lambda_0$  for each thermodynamic condition is denoted by  $\lambda_0(\rho_s, T_s)$  and is chosen to minimize the error in pressure  $E = |P_{\text{sim}}(\rho_s, T_s) - P_{\text{ref},s}|$  independently for each density  $\rho_s$ . We use here a non-dependent potential taking a constant value of  $\lambda_0$  in (11) and run simulations in the NVT ensemble during an integration time  $t_{\text{sim}} = 1 \text{ ns}$  to obtain  $P_{\text{sim}}(\rho_s, T_s)$ . The pressures resulting from this

first optimization, displayed as orange squares in Figure 9 and labeled as 'independent optimization', are by construction almost on top of reference data.

Figure 8 presents the values of  $\lambda_0$  as a function of  $V_s = \frac{m_{\text{sys}}}{\rho_s}$ . This suggests to interpolate the values of  $r_0$  by a polynomial fit. A quadratic least-square fit is displayed in Figure 8.

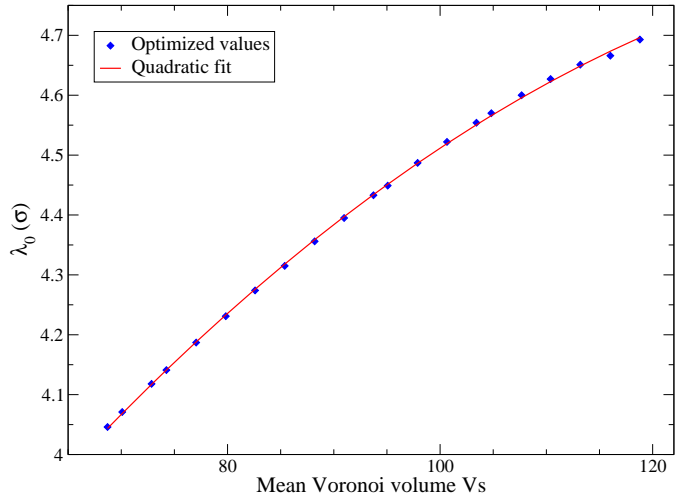


FIG. 8: Optimal  $\lambda_0$  for the reference states with respect to the mean Voronoi volume  $V_s = \frac{m_{\text{sys}}}{\rho_s}$

##### B. Optimized distance correction

We now fit the distance correction on the whole set of thermodynamic states  $(\rho_s, T_s)_{1 \leq s \leq N_s}$  by a polynomial function of degree  $p$ :

$$\lambda(V) = \sum_{i=0}^p a_i V^i. \quad (12)$$

The coefficients  $\{a_i\}$  are chosen in order to minimize the mean quadratic error in pressure:

$$F(\{a_i\}) = \sqrt{\frac{1}{N_{\text{ts}}} \sum_{s=1}^{N_{\text{ts}}} (P_{\text{sim}}(\rho_s, T_s) - P_{\text{ref},s})^2}.$$

In this expression,  $P_{\text{sim}}(\rho_s, T_s)$  is the average pressure in the NVT ensemble at density  $\rho_s$  and temperature  $T_s$  for the potential energy function (7) with the distance correction (12). We carry out the minimization of this quadratic error  $F$  with a Newton algorithm. The first and second order derivatives of  $F$  are approximated by computing the canonical average of the observables obtained by differentiating the pressure observable with respect to the coefficients  $\{a_i\}$ . The initial guess for the values of

$\{a_i\}$  is obtained by a least-square fit based on Figure 8. Note that the parameter  $\lambda$  decrease when the density increases (or equivalently as the Voronoi volume decrease), which is indeed the expected physical behavior discussed at the beginning of Section III A. Consistently with the observations made in Section III C, directly using this initial guess leads to poor results since the pressure is largely underestimated. The optimization procedure to minimize the mean quadratic error  $F(\{a_i\})$  is therefore mandatory:

- We first show that it is impossible to reproduce the correct pressure by using the same constant, non-dependent  $\lambda_0$  for every density  $\rho_s$  (which corresponds to  $p = 0$  in (12)). The minimization of  $F$  yields  $a_{0,\min} = 4.0588 \sigma$  and  $F(a_{0,\min}) = 3.131$  GPa (filled circles in Figure 9). This is a prohibitively large error, revealing a poor agreement with the reference curve. The brutal increase in pressure at  $\rho \approx 1900 \text{ kg.m}^{-3}$  clearly underlines the non-transferability of the non-dependent potential ( $p = 0$ ) to a large set of thermodynamic states. This shows that we need to consider genuinely density dependent potentials, namely  $p \geq 1$ .
- The minimization of  $F$  as a function of  $(a_0, a_1)$  when  $p = 1$  gives  $a_{0,\min} = 3.1886 \sigma$  and  $a_{1,\min} = 1.3420 \cdot 10^{-2} \sigma^{-2}$  with an error  $F(a_{0,\min}, a_{1,\min}) = 1.396$  GPa. Although lower than with  $p = 0$ , such a large error still means the computed Hugoniot curve (blue triangles in Figure 9) largely deviates from the reference curve, with too large a curvature. This suggest to further increase the degree of the polynomial  $\lambda(V)$ .
- The minimization of a quadratic distance correction  $\lambda$  ( $p = 2$ ) leads to  $a_{0,\min} = 2.4784 \sigma$ ,  $a_{1,\min} = 3.1095 \cdot 10^{-2} \sigma^{-2}$  and  $a_{2,\min} = -1.0247 \cdot 10^{-4} \sigma^{-5}$ . The corresponding error  $F(a_{0,\min}, a_{1,\min}, a_{2,\min}) = 0.034$  GPa shows an almost perfect agreement between the reference Hugoniot and the predicted one (red diamonds in Figure 9).

We show in Appendix D that our density dependent potential provides satisfactory results at even larger densities and pressures without carrying another optimization to include these thermodynamic states in the optimization set. This can be seen as some transferability property.

## V. CONCLUSION

We have proposed a method to model the compressibility of mesoparticles representing a large collection of molecules. This method ensures that accurate thermodynamics properties (i.e. Equation of State) can be preserved during the coarse graining process of molecular systems. As the scale of the modelling increases, two

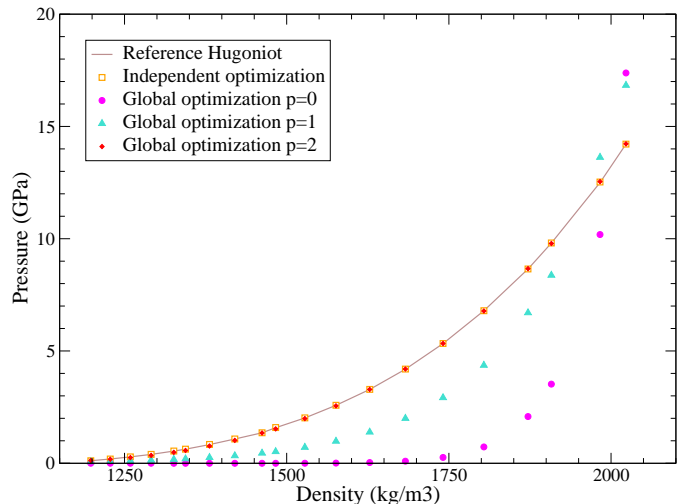


FIG. 9: Hugoniot curve for nitromethane: reference curve [21] and results for density-dependent potentials with  $p = 0$  and  $p = 2$ .

additional terms, namely the thermic and the cold (pressure) contributions of coarse grained degrees of freedom, have to be taken into account for the computation of the total energy. None of these terms appear in the original DPD framework. The thermic contribution appeared later, as non-equilibrium situations of mesoparticles were considered. The second term, the internal compressibility of mesoparticle, has been implicitly neglected when coarse graining single molecules, or when the thermodynamic domain of interest remains near standard conditions. This term becomes significant when several molecules are embedded in a single mesoparticle, and when a large range of pressures and densities is targeted.

We explored the possibility of modelling the compressibility of mesoparticles by introducing a local dependence in our potential. Two local quantities were studied to that purpose: a spherical local density within a cut-off radius and a volume defined by a Voronoi tessellation. Introducing a dependence of either of these local quantities in the interaction potential, we noticed a significant increase of pressure in our simulations. This increase has to be accounted for when fitting density dependent potentials to reproduce Hugoniot curves for nitromethane mesoparticles. Finally, we managed to accurately reproduce the Hugoniot curve of model nitromethane for mesoparticles containing thousand molecules. For this resolution, a gain of several order of magnitude in the CPU time is obtained both from the increase in the integration timestep and from the lower number of interactions.

## Appendix A: Langevin dynamics

To carry out simulations in the NVT ensemble, we resort to Langevin dynamics. Given a potential energy function  $\mathcal{U}_{\text{tot}}(q)$ , the equations of motion read

$$\begin{aligned} dq_t &= \frac{p_t}{m} dt \\ dp_t &= -\nabla \mathcal{U}_{\text{tot}}(q_t) dt - \gamma \frac{p_t}{m} dt + \sqrt{\frac{2\gamma}{\beta}} dW_t, \end{aligned}$$

where  $\gamma > 0$  is the friction parameter and  $W_t$  is a standard Brownian motion. We discretize here the Langevin dynamics by splitting the Hamiltonian part of the dynamic and the thermostat part. We use a velocity-Verlet integration scheme for the Hamiltonian part, and integrate analytically the thermostat part (see [22] for a numerical analysis of the error on the invariant measure). This gives the following scheme:

$$\begin{cases} \tilde{\mathbf{p}}_i^{n+1/2} = \mathbf{p}_i^n - \nabla_{\mathbf{q}_i} \mathcal{U}_{\text{tot}}(\mathbf{q}^n) \frac{\Delta t}{2}, \\ \mathbf{q}_i^{n+1} = \mathbf{q}_i^n + \frac{\mathbf{p}_i^{n+1/2}}{m} \Delta t, \\ \tilde{\mathbf{p}}_i^{n+1} = \mathbf{p}_i^{n+1/2} - \nabla_{\mathbf{q}_i} \mathcal{U}_{\text{tot}}(\mathbf{q}^{n+1}) \frac{\Delta t}{2}, \\ \mathbf{p}_i^{n+1} = \exp(-\gamma \Delta t) \tilde{\mathbf{p}}_i^{n+1} + \sqrt{\frac{m(1 - \exp(-2\gamma \Delta t))}{\beta}} G_i^n, \end{cases}$$

where  $(G_i^n)_{i,n}$  are independent standard normal variables.

In the reduced units defined by the mass  $m$  of a particle, the length scale  $\sigma$  and the energy scale  $\varepsilon$  in (11), the friction parameter is chosen to be  $\gamma = 1$ , while the time step is  $\Delta t = 0.001$ .

### Appendix B: Harmonic mean of the spherical local density

Since we define the average Voronoi density through a harmonic mean, it is fair to look at the behavior of the spherical densities under harmonic averages. Figure 10 presents the evolution of the harmonic mean spherical density as a function of the cut-off radius for the weight functions studied in Section II A. The harmonic mean clearly presents the same issues as the arithmetic mean of the spherical density, namely a bias in the mean spherical density.

### Appendix C: Local density dependent Lennard-Jones potential

We explore in this section another general example of density dependent potential based on a reference potential  $\mathcal{U}_{\text{std}}$ . In contrast to (7), it is possible to introduce a

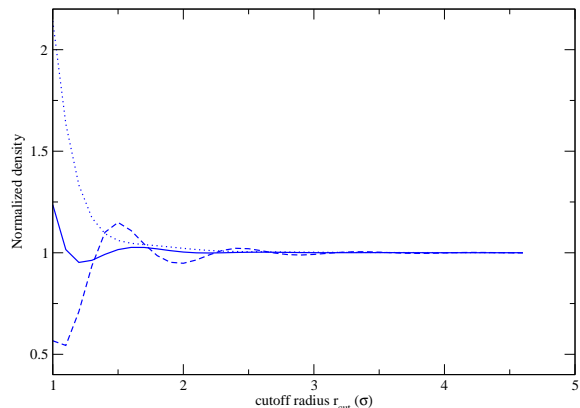


FIG. 10: Harmonic mean local density for the Lucy function (dotted line), the smoothed step function (dashed line) and the cubic spline (solid line).

volume dependence by rescaling the distances:

$$\mathcal{U}_{\text{dd}}(r_{i,j}, V_{i,j}) = \mathcal{U}_{\text{std}}\left(\frac{l_0}{l_{i,j}} r_{i,j}\right),$$

where  $l_{i,j} = l(V_{i,j})$ . A relevant example for this kind of dependent potential would be a Lennard-Jones potential where the length scale becomes dependent on the local density in a way which ensures that  $l_0 = l_{\text{std}}$ , the length scale for the standard Lennard-Jones potential.

As in Section III, the introduction of a dependence on the Voronoi volume in the potential naturally causes extra forces to appear when deriving the potential energy.

$$\begin{aligned} \mathbf{F}_{\text{dd}}^{i,j,k} &= -\nabla_{\mathbf{q}_k} \mathcal{U}_{\text{dd}}(r_{i,j}, V_{i,j}) \\ &= \left( (\delta_{k,i} - \delta_{k,j}) \mathbf{e}_{i,j} + \frac{l'(V_{i,j})}{l_{i,j}} r_{i,j} \nabla_{\mathbf{q}_k} V_{i,j} \right) \times \\ &\quad \frac{l_0}{l_{i,j}} \mathcal{U}'_{\text{std}}\left(\frac{l_0}{l_{i,j}} r_{i,j}\right). \end{aligned}$$

As in (9), the contribution to the virial pressure of the interaction between particles  $i$  and  $j$  is altered by these extra forces:

$$\begin{aligned} w_{\text{dd}}^{i,j} &= \sum_k \mathbf{F}_{\mu}^{i,j,k} \cdot \mathbf{q}_k \\ &= w_{\text{direct}}^{i,j} \left( 1 - \sum_k \frac{l'(V_{i,j})}{2l_{i,j}} \nabla_{\mathbf{q}_k} (V_i + V_j) \cdot \mathbf{q}_k \right), \end{aligned}$$

where  $w_{\text{direct}}^{i,j} = -\frac{l_0}{l_{i,j}} \mathcal{U}'_{\text{std}}\left(r_{i,j} \frac{l_0}{l_{i,j}}\right) r_{i,j}$ . Using (5), we finally obtain (compare (9))

$$w_{\text{dd}}^{i,j} = w_{\text{direct}}^{i,j} \left( 1 - \frac{3l'(V_{i,j})V_{i,j}}{l_{i,j}} \right).$$

### Appendix D: Test of the density dependent potential outside the optimization range

We study the ability of our density dependent potential to predict the correct pressure for densities outside the optimization range (here  $1170 \text{ kg.m}^{-3} \leq \rho_s \leq 2023 \text{ kg.m}^{-3}$ ). We use a quadratic distance correction  $\lambda$  with the parameters optimized used to produce the results of Figure 9. We test the potential on a new set of  $N_{\text{test}}$  thermodynamic states indexed by  $k$  ( $2100 \text{ kg.m}^{-3} \leq \rho_{\text{test},k} \leq 2350 \text{ kg.m}^{-3}$ ) by estimating the relative mean quadratic error

$$F_{\text{test}}(\{a_i\}) = \sqrt{\frac{1}{N_{\text{test}}} \sum_{k=1}^{N_{\text{test}}} \frac{(P_{\text{sim}}(\rho_{\text{test},k}, T_{\text{test},k}) - P_{\text{ref},k})^2}{P_{\text{ref},k}}}$$

The relative error on the test set of thermodynamic states  $F_{\text{test}} = 0.015$  is larger than the error on the optimization set ( $F = 0.002$ ), but the computed results are still in excellent agreement with the reference Hugoniot curve as shown in Figure 11.

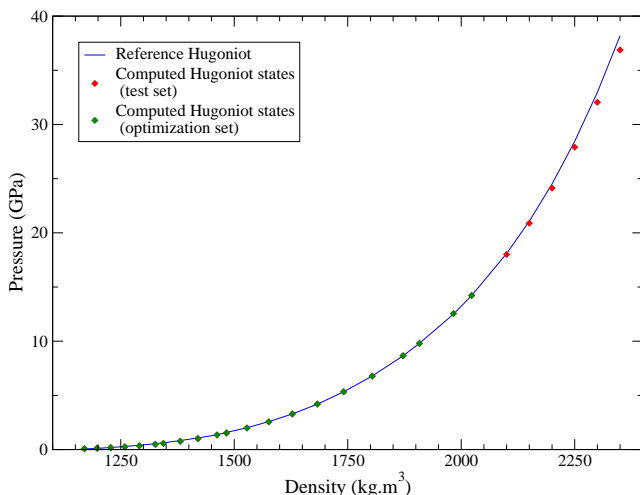


FIG. 11: Hugoniot curve for nitromethane: Predicted values of the pressure outside the optimization range of the parameters.

- 
- [1] Hoogerbrugge P.J. and Koelman J.M.V., *Europhys. Lett.*, 19, 155, 1992.
  - [2] Flekkøy E.G., Coveney P.V. and De Fabritiis G., *Phys. Rev. E*, 62, 2140, 2000.
  - [3] Español P. and Warren P., *Europhys. Lett.*, 30, 191, 1995.
  - [4] Español P., *Europhys. Lett.*, 40, 631, 1997.
  - [5] Avalos J.B. and Mackie A.D., *Europhys. Lett.*, 40, 141, 1997.
  - [6] Strachan A. and Holian B.L., *Phys. Rev. Lett.*, 94, 014301, 2005.
  - [7] Stoltz G., *Europhys. Lett.*, 76, 849, 2006.
  - [8] Tersoff J., *Phys. Rev. Lett.*, 56, 632, 1986.
  - [9] Daw M.S. and Baskes M.I., *Phys. Rev. B*, 29, 6443, 1984.
  - [10] Louis A., *J. Phys.:Condens. Matter*, 14, 9187, 2002.
  - [11] Merabia S. and Pagonabarraga I., *J. Chem. Phys.*, 127(5), 054903, 2007.

- [12] Izvekov S., Chung P.W. and Rice B.M., *J. Chem. Phys.*, 133, 064109, 2010.
- [13] Izvekov S., Chung P.W. and Rice B.M., *J. Chem. Phys.*, 135(4), 044112, 2011.
- [14] Lucy L.B., *Astron. J.*, 82, 1013, 1977.
- [15] Almarza N.G., Lomba E., Ruiz G. and Tejero C.F., *Phys. Rev. E*, 67, 021202, 2003.
- [16] Serrano M., De Fabritis G., Español P., Flekkoy E. and Coveney P., *J. Phys. A: Math. Gen.*, 35, 1605, 2002.
- [17] Serrano M. and Español P., *Phys. Rev. E*, 64, 046115, 2001.
- [18] Johnson M.E., Head-Gordon T. and Louis A.A., *J. Chem. Phys.*, 126, 144509, 2007.
- [19] Rycroft C.H., *Chaos*, 19(4), 041111, 2009.
- [20] Maillet, J. B., Bourasseau, E., Desbiens, N., Vallverdu, G. and Stoltz, G., *Europhys. Lett.*, 96(6), 68007, 2011.
- [21] Desbiens N., Bourasseau E., Maillet J.B. and Soulard L., *J. Hazard. Mater.*, 166, 1120, 2009.
- [22] Leimkuhler B., Matthews C. and Stoltz G., *arXiv preprint*, 1308.5814, 2013.